MINISTRY OF AVIATION SUPPLY

AERONAUTICAL RESEARCH COUNCIL

REPORTS AND MEMORANDA

A Three Component Gun Tunnel Balance Designed for Testing Thin Delta Wings

By T. OPATOWSKI
Ph.D., D.C.Ae., C.Eng., A.F.R.Ae.S.

Dept. of Aeronautics, Imperial College

A Three Component Gun Tunnel Balance Designed for Testing Thin Delta Wings

By T. OPATOWSKI
Ph.D., D.C.Ae., C.Eng., A.F.R.Ae.S.

Dept. of Aeronautics, Imperial College

Summary.

The design, development and performance of a three component strain gauge balance system designed for testing thin wings in the Imperial College gun tunnel is described. The balance was machined out of high strength steel and employed miniature silicon strain gauges on tension and compression links in order to meet the difficult strength/stiffness requirements. Natural frequencies were attenuated with 'parallel T' filters.

Various problems which arose in its development were successfully overcome and some excellent results were obtained.

LIST OF CONTENTS

---

5. Development and Calibration

    5.1.   Initial results and modifications

    5.2.   Static calibration, direct

    5.3.   Interaction

    5.4.   Natural frequencies

    5.5.   Filter attenuation and response

    5.6.   Tare calibrations

    5.7.   Hemisphere check

6. Performance and Accuracy

    6.1.   Performance

    6.2.   Accuracy

    6.3.   Some results obtained with the balance

7. Discussion and Conclusions

8. Acknowledgements

References

Illustrations—Figs. 1 to 17

LIST OF ILLUSTRATIONS

1. Introduction.

The work reported here was part of a continuing programme of force measurements on wings and bodies in the Imperial College gun tunnel and forms part of a thesis for the degree of Ph.D. submitted to London University[9].

The Balance described in this report is termed MK 3 as there was a previous balance (MK 2)[7] which in turn was a highly modified form of an earlier balance. The MK 2 balance had only limited usefulness. The MK 3 balance was designed specifically to mount the thinnest possible delta wings having high lift/drag ratios. Ancillary design aims were greater accuracy, wider range of tunnel conditions in which the balance could be used, greater sensitivity, higher natural frequencies and smaller interactions.

Since the balance was to be entirely new, the opportunity was taken to design a complete balance system incorporating means for setting incidence and roll and for calibrating the balance both in and out of the tunnel.

In the event, nearly all the design aims were achieved. However, there were some difficulties which complicated the operation of the balance and the reduction of the results (*See* Ref. 9).

Any assessment of the quality of measured forces must include the effects of flow field characteristics and so some details of the calibration of the Mach 8·3 contoured nozzle have been included. One item of comparative novelty was a 'pressure recovery' flow inclination probe which proved to be highly sensitive.

2. Tunnel Calibration.

2.1. Nozzle Details.

The contoured nozzle was made of resin-bonded fibreglass except for a section near the throat which was made of light alloy and into which a stainless steel throat insert was screwed.

The nozzle design and construction was executed by Bristol Siddeley Engines Limited. The method of I. M. Hall[1] was used to determine the transonic flow characteristics of the constant radius throat to a Mach number of 1·05 to 1·1, thus giving a starting line for the characteristics solution. The Mach number distribution along the nozzle axis was specified in the form of a conic fitted to the Mach number and first and second derivatives at the starting line and Mach number and zero gradient at the exit. The maximum divergence half-angle was 21·7°, close to the maximum possible of 24°, in order to keep the nozzle as short as possible. The resulting contour was corrected for boundary-layer growth, the correction being based on Stratford and Beavers[2] assuming zero thickness at the throat with turbulent flow everywhere downstream and zero heat transfer.

2.2. Pitot Pressure Survey.

A full description of the tunnel and calibration of the driver section is given by Needham in Ref. 3. A special pitot rake capable of being traversed along and across the working section was built for the calibration.

The measured pitot pressures have been converted to values of Mach number using the Rayleigh pitot formula, assuming isentropic expansion from the stagnation conditions of Ref. 3.

2.3. Mach Number Distribution Results.

The results of the longitudinal survey at normal barrel pressure are plotted in terms of Mach number in Fig. 1a and a lateral cross section at 3 in aft of the exit plane in Fig. 1b.

The results with the barrel pressurized are tabulated below. In this condition the pressure trace was not constant in the first wave and gave a slightly different answer in the second and subsequent waves. Typical traces are shown in Figs. 2.

4

Distance from Centreline	Exit plane	Mach No.	
		3 in AFT	6 in AFT
0·5 in UP	8·18	8·26	8·22
	8·32	8·35	8·35
1·5 in UP	8·12	8·16	8·14
	8·21	8·23	8·28
2·5 in UP	8·12	8·19	8·19
	8·21	8·25	8·28
CENTRELINE	7·965	8·13	8·025
	8·21	8·18	8·14
1 in DOWN	8·11	8·11	8·19
	8·22	8·15	8·25
2 in DOWN	8·17	8·25	8·17
	8·3	8·28	8·26
3 in DOWN	8·09	8·12	
	8·17	8·17	

Upper value is first wave and the lower second and subsequent waves.

The accuracy of the results is estimated to be about equivalent to $\pm 0.1 M_N$ though the lines in Fig. 1 have been drawn through the measured points (or means position where more than one reading was taken).

Measurements were taken on the centreline and 0·5 in above it and this latter point has been reflected about the centreline in order to facilitate the drawing of the curve in this region of large variations. Fig. 1 shows clearly the focusing effect of the axially symmetric nozzle, and it is probable that the fluctuations are even more localised to the centre than drawn.

Other than on the centre, within the accuracy of the tests, the flow was sensibly steady at a Mach number of about 8·25. This is borne out by the lateral distribution shown in Fig. 1b.

The results with the barrel pressurized were very similar to those for normal pressure. Hemisphere drag measurements showed that the Mach number when running pressurized was nearer 8·3 and this value has been used where appropriate.

Schlieren photographs taken of the flow in both conditions were entirely normal and showed no obvious discontinuities.

The running time in normal operation $\left(\dfrac{\text{driver pressure}}{\text{barrel pressure}} = 136 \right)$ as taken from the traces was about 28 milliseconds.

2.4. Flow Inclination.

An incidence probe was built in order to check the inclination of the flow relative to the floor of the tunnel working section. This was of the blunted cone 'pressure recovery' type (e.g. Album[4]) in which the differential pressure from two pitot tubes embedded in the entropy layer of a blunted cone is used as an indication of flow incidence. The probe is shown in Fig. 3a and a schlieren photograph of the flow about it in Fig. 3b. The cone diameter was 0·5 in, tip diameter 0·08 in and included angle 30°.

The probe was experimentally developed and calibrated. To obtain satisfactory characteristics the cone had its blunting increased until the desired characteristics were obtained. It was calibrated by rotating the sensing head through 180° to determine the zero error and by varying the incidence at one location

(measured by 'clocking' the height from the working section floor to datum surfaces at front and rear of the probe) to determine the sensitivity to flow inclination.

Results obtained at a position 1 in below the centreline and 3 in from the exit plane are presented in Fig. 4. The sensitivity near zero inclination was 14 psi/degree inclination or in terms of pressure coefficient, $2.3/°$. The flow was parallel to the working section floor to within $0.1°$.

2.5. *Repeatability.*

As an indication of the repeatability of the tunnel, one measurement was repeated several times during the calibration of the nozzle. A repeatability of 97% over 6 runs was achieved. Since these runs included instrumentation errors, the variation due to changes in tunnel running conditions would be expected to be less than $\pm 3\%$.

3. *Balance Design Considerations.*
3.1. *General.*

There are many factors to be considered in the design of a balance, some are applicable to all wind-tunnel balances and others are unique to gun-tunnel (or even more critically to shock tunnel) applications. For convenience and also in order to demonstrate the scope of the problem, they are listed below:

> high natural frequency
>
> sensitivity
>
> small size and frontal area
>
> accuracy
>
> ease of calibration
>
> low interactions
>
> strength
>
> incidence accuracy and range
>
> compatibility with tunnel and models
>
> ability to be produced in time and cost
>
> reliability.

In general, the forces applied by the airstream to the model are reacted by a combination of inertia and support forces. Inertial forces arise both from the model and from parts of the balance (and supporting structure) while the remaining forces are reacted by the balance and constitute its output. Thus the error that the inertia forces represent must either be measured and added to the result or allowed for in some other way. The various system stiffnesses can be such that the proportion of inertia force to support force varies from all inertia, through various proportions to virtually all support. At the one extreme, forces are derived from measurements (usually but not necessarily photographic) of acceleration on free flying or very lightly supported models[5]. In the central range are inertia compensated balances while at the latter end of the range are the more usual, uncompensated balances with various ways of dealing with the residual oscillations.

Only balances incorporating accelerometers are capable of giving a true instantaneous measurement of the force on a model. All the others give an average over some period of time and the problem is to make this period short enough in relation to the characteristics of the tunnel for which the balance is intended.

Each type of balance has its problems. It is very difficult to control or measure the incidence of models when they are only lightly supported and the measurements of acceleration is also not very accurate in these circumstances. One major advantage of this type of measurement is that sting interference effects

are entirely absent, though this makes the measurement of base pressure for correction purposes very much more difficult. The inertia compensated balance on the other hand, while inherently the most versatile and accurate, is complicated, expensive and difficult to calibrate. While good results have been obtained with both the above types of measurement, it was thought preferable to continue development of the existing type of balance rather than change to a new type.

The main problem therefore was that of obtaining a true average reading in the available time. A recent development that promises a considerable improvement in this type of measurement is the use of field effect transistors (F.E.T.) with piezo-electric transducers[6]. The F.E.T.'s appear to eliminate many of the problems associated with the use of these highly stiff transducers as well as giving a useful amplification of the signal.

3.2. *Design Principles of the MK 3 Balance.*

Most of the requirements are conflicting and any improvement in one attribute is usually obtained only at the expense of another. In the present (MK 3) balance, four important design features gave improvements which could be shared between the conflicting requirement. These were: use of high strength steel, tension link sensing elements, silicon gauges and the layout of the sensing elements.

The high strength steel, (details of which are given in Section 4.1) enabled the sting size to be brought down to 0·25 in diameter, making 6° thick models possible for the 5 in long models used.

The use of tension links in place of the more usual cantilevers for sensing elements, can give more than five times the stiffness for the same sensitivity, even when compared to the shortest practical cantilever. This is a direct gain to the performance of a balance. The only problem, for the order of loads available, was that the links were so thin that their strength in buckling was critical. This required the use of miniature gauges (with some associated unreliability) in order to keep the link lengths short.

The considerable increase in sensitivity available from silicon gauges (and their associated problems) have already been discussed in Ref. 7. These problems are less with the normal foil and wire gauges and, though expensive, good d.c. amplification is available. However, one important consideration is the signal to noise ratio, as any noise originating before the amplifier will also be amplified. With the existing electrical environment it was felt safer (and cheaper) to rely on a high gauge output than on subsequent amplification.

In Appendix B of Ref. 7 it is shown that the accuracy of measurement of pitching moment is highly dependent on the distance between the point of measurements and the centre of pressure. An accurate knowledge of the position of the centre of pressure is also needed in deriving the value of the lift force. Thus it is of paramount importance that the moment sensor should be buried in the model, close to the C.P. and if this is so, the lift and drag can be measured behind the model with little loss of accuracy. (It is possible to reduce the sensitivity to C.P. position by a parallelogram linkage but at the expense of an increase in the bulk and in the difficulty of manufacture, e.g. *see* Ref. 8).

The above comments have indicated the philosophy behind the design; Section 4 below describes the balance in detail.

4. *Description of Balance and Associated Equipment.*

4.1. *The Balance 'Plug-in' Unit.*

The main part of the balance containing all the active elements is shown with covers off in Fig. 6.

The models were screwed onto thread A and located by the spigot B and taper C. Two gauges, measuring pitching moment, were cemented onto the flats D and the leads from them ran back in channels E (one each side). The gauges and wires were cemented over to give a smooth 0·25 in diameter cylindrical sting.

Lift was measured by four gauges stuck, one on each surface of the two tension links F, each of which was 0·010 in thick. Drag was measured by a similar arrangement on the links G.

The wiring between upper and lower lift gauges and between the gauges and the 15-way miniature McMurdo plug J, was by means of two printed circuits* H, one each side of the balance.

The whole balance unit was bolted to the incidence gear by a bolt K and locating pin L. The shield M had a replaceable portion N screwed into it, to cater for different length models.

In its original form the balance had light covers screwed onto each side but these were changed to

---

*These circuit boards were made at Imperial College by the departmental photographer, Mr. O'Leary.

0·125 in gauge plate and attached by taper pins in order to reduce the lift interaction on drag. Finally, since the balance proved sensitive to loads on its external structure, a separate wind shield was added.

The main part of the balance, (parts A to L inclusive) was machined out of a single piece of EN 24W steel, heat treated to a Brinell hardness number of 320 and giving an ultimate strength of 70 tons/sq in.

4.2. *Incidence Adjustment.*

For incidence adjustment the balance unit was bolted onto the linkage shown in Fig. 7a. By sliding the top and bottom plates horizontally in the existing channels of the gun tunnel the unit was made to rotate about the upper pivot point which was so placed as to give the least vertical movement of the model centre of pressure. The vertical movement was about 0·25 in through the incidence range of 0 to 30° (available range ± 30°).

The attachment shown dotted on Fig. 7, which was held by two pins registering in accurately located holes, enabled the incidence to be set by means of an inclinometer to within 2 minutes. The attachment could also be located with the horizontal bar across the tunnel in order to set the position of the model in roll. The final position of a model in roll was determined by the position of the taper on the sting. If the model position was not correct it could be adjusted by relieving the taper in the model with a special tool, or by inserting thin paper washers. The edge of the incidence attachment also served as a datum from which horizontal distances were measured.

The balance was so stiff that there was negligible change of incidence with the loads of the present tests.

4.3. *Circuit Arrangement.*

A complete circuit diagram is given in Fig. 8. The gauges were miniature silicon gauges, type 2A-3A-120P, supplied by Ether Ltd. These were chosen in preference to more sophisticated gauges, (smaller size, better temperature characteristics) which are obtainable from the U.S.A., because they were more readily available. Several had to be replaced.

The gauges were arranged in conventional Wheatstone bridges; full bridges for lift and drag and, because of limited space, a single active leg with dummy second leg for the pitching moment as shown in Fig. 5. They were supplied from a common 3v stabilized voltage source (Farnwell Instruments Ltd.) but with individual return leads. By keeping the supply voltage down to 3v the self heating was reduced to negligible proportions. Inserted in each return lead was a small calibration resistor the voltage across which was a measure of the current through the corresponding bridge and hence of the bridge total resistance. To avoid errors, the balancing circuits were disconnected from the bridges before the voltages across these resistors were measured.

All setting up and calibration measurements were made using a Solartron 1420 digital voltmeter. This was used for balancing the circuits, taking readings on calibration, measuring the value of the stabilized voltage, and the voltages across the calibration resistors. These latter resistors were used to compensate for the effect of temperature on the silicon gauges in the same manner as described in Ref. 7, except that all the gauges of a bridge were taken together and assumed to be at equal temperature.

Balance outputs during tunnel runs were displayed on a Tektronix 502 oscilloscope and recorded with a Land Polaroid camera.

4.4. *Filter Units.*

In its original form, the balance was fitted with conventional low-pass filters on each channel. These eliminated much of the noise and gave some 30 per cent attenuation to natural frequencies of around 200 cycles/sec. When this type of filtering was increased to the point where the maximum permitted rise time was obtained—about 15–20 m/sec—about 70% of the oscillating component could be removed. Subsequently some parallel T or 'notch' filters were added and the low-pass filters time constants reduced to keep the rise time below the permitted limit.

The parallel T filter (shown in Fig. 9a in its most usual form) is capable of being tuned to give an infinite impedance to a particular frequency given by:

$$f = \frac{1}{2\pi R_1 C_1} \tag{1}$$

for zero load.

The actual achieved performance depends on the quality and matching of the components and on the loading conditions. These filters work from a low impedance into a high one.

Commercial notch filters all seemed to have one side earthed and this proved to be incompatible with the balance and with the rest of the electronics. Some special filters were therefore constructed (Fig. 9b), being tuned to the known frequency of the balance. These were originally adjustable to several frequencies but this feature was dropped as it caused considerable noise pick-up.

Despite the lack of component matching, between 95 per cent and 98 per cent of the oscillatory component could be removed at the tuned frequency, with a fairly rapid drop-off of performance with frequency away from the optimum.

4.5. *Calibration Equipment.*

The calibration set-up for static calibration and for dynamic interaction is shown in Fig. 7b. The equipment could be used *in-situ* in the tunnel in both cases.

Lift and moment were calibrated by direct application of weights, hung from the grooves of the calibration bar shown. For drag, the special bracket was pinned onto the incidence gear and the drag load applied *via* a 2:1 bell crank, supported on knife edges. This mechanical advantage enabled high loads to be achieved in the restricted space of the tunnel. The drag linkage was levelled by the pointed screw at the front. Because of the high rigidity of the balance, it was not necessary to compensate or allow for the deflection under load on calibration. (The deflection under lift load was 5×10^{-4} in/lb at the tip of the balance and about 4×10^{-6} in/lb for drag).

Fig. 7b shows the arrangement for calibrating the interaction of lift on drag under dynamic loading. For this, the lift and drag outputs were fed to the x and y plates of an oscilloscope with appropriate amplifications and produced a line whose slope was proportional to the interaction. With this system the interaction could be determined to 0·2 per cent. To ensure that no interaction was being fed in by the calibration mechanism, the loading bar A was raised until the drop arm B had found its own vertical. The loading bar was then lowered onto the spherical nut at the bottom of the drop arm which had been previously set to make the loading bar horizontal. Weights were dropped by hand onto the loading platform at the front of the loading bar.

5. *Development and Calibration.*

5.1. *Initial Results and Modifications.*

Some of the problems encountered are described below as it is felt that the information could be useful to others in assessing the possibilities and usefulness of this type of design.

The first problem encountered was one of inconsistency in the bridge balance points and the lift interaction on drag which was non-linear and varied from time to time from near zero to 14 per cent. This was coupled to an extreme sensitivity to loads on the external structure. The trouble was traced to variations in the strength of attachment (screw tightening) of the side covers. Without the covers the interaction was consistently -14%. It would seem that the tension links were so stiff and sensitive that the supporting structure was not sufficiently rigid in comparison and fed loads back into the drag channel. The only solution available was to replace the side covers by load-carrying side plates which were held by taper pins to minimize any lost movement. These reduced the static interactions to less than 1% and consistent results were obtained. The sensitivity to external loads was also reduced, though not eliminated.

Apart from the difficulty of access to the internals of the balance, the taper pinned side covers were not entirely satisfactory as they introduced a possible source of non-linearity, hysteresis and temperature sensitivity. The latter effect could be dealt with by the existing temperature calibration procedure but the

first two effects made a dynamic calibration to measure interactions a necessity.

Since the tension links also acted as flextures, a certain amount of interaction on individual gauges was expected. This was expected to be small because of the high stiffness of the balance and any remaining interaction was to be balanced out by the bridge arrangement of the gauges. Because of the fixed ends, the links deflected in an 'S' shape and hence it was possible to obtain variations of interaction on any particular gauge depending on precisely where it was positioned along the length of the link. This arrangement produced unexpected interactions but also provided a mechanism by which any desired variation of interaction could be achieved. To take advantage of this, a rig was constructed by which the output of any individual gauge could be measured. This was merely inserted in series with the output of the balance and proved useful in tracing faulty gauges and indicating which gauges to move in reducing interaction.

The principle of operation of the apparatus was simply that in any leg of a bridge the companion gauge to the one being examined was shorted out by a small resistor and the voltage change across this resistor was then a direct indication of the resistance change of the subject gauge. The supply voltage was adjusted to give the correct current through the subject gauge.

An additional problem was that calibrations performed outside the tunnel differed from those obtained *in-situ* and there were some inconsistencies in the calibrations obtained in the tunnel. These variations were traced to variations in resistance of connecting cables and connectors. Consistency for *in-situ* calibrations was obtained by putting the temperature calibration resistors in a box in the tunnel and taking all voltage measurements from this point. Thermoelectric effects were also reduced by increasing the size of these resistors. However, external calibrations could not be directly related to *in-situ* calibrations and only the latter could be used for test results. The relationship between sensitivity and reading of the temperature calibration resistor was still not entirely consistent but the temperature varied little and the problem was overcome by frequent calibration.

5.2. *Static Calibration, Direct.*

The more comprehensive calibrations for linearity and the effect of temperature were carried out on the calibration rig with rather briefer checks in the tunnel. Figs. 10 show results obtained on the rig, for lift, drag, and pitching moment. The calibration was linear on all channels.

Also shown on the figures is the variation of sensitivity with temperature. This variation was used with the *in-situ* calibrations for reducing the results. The fact that the temperature sensitivity of the drag channel was of opposite sign to that of the other two channels suggests a variation in the gauge characteristics, probably in those used for the drag measurement. During the period of the tests the lift and moment channels were consistent throughout and though the temperature correction on the drag channel was a little inconsistent, the corrections due to temperature on the drag channel were less than 1 per cent.

The sensitivities obtained from the *in-situ* calibrations and the temperature corrections used are summarized below:

Channel	Datum resistance reading	Sensitivity at $V = 2.91$ volts	% Change in sensitivity per 1% change of resistance
Moment	1696	0·195 lb/mv	−0·6
Lift $\left(L + \dfrac{M}{4\cdot 5} \right)$	1725	0·274 lb/mv	−2·5
Drag	1755	$\dfrac{0\cdot548}{0\cdot575}$ lb/mv	+0·8

where V is the applied voltage as measured at the balance, having dropped from 3·02 at the voltage source in passing through the cables and connectors.

The method of obtaining the lift from the readings was the same as that used with the first (MK 2) balance and given in Appendix B of Ref. 7.

5.3. Interaction.

Measurements of interaction under static loading were made between all channels and both in the loaded and unloaded conditions. These calibrations were carried out on the calibration stand. The interactions, which are tabulated on the following page, were so small that it was not possible to determine linearity. There was no change as between loaded and unloaded conditions.

Effect of	on	Interaction
Lift	Drag	−0·8% at zero moment
Drag	Lift	−0·9%
Lift	Moment	Included in normal calibration curves.
Moment	Lift	Included in normal calibration curves.
Drag	Moment	Zero
Moment	Drag	Included in normal calibration.

The lift interaction on drag varied with the position of application of the lift load but as the C.P. for the tests was known to be very close to the zero moment position, only this condition was taken.

As the proportion of vibration being fed through from the lift to the drag channel seemed higher than could be accounted for from the above figures, it was decided to carry out a dynamic interaction calibration. This was accomplished by the method described in Section 4.5, with the following results:

Lift on drag	−2 to −2·5%
Drag on lift	−0·9%

The dynamic interaction of the lift on drag channel appeared to decrease slightly throughout the period of the tests as can be seen by the range quoted.

Typical dynamic interaction traces are shown in Fig. 11. The vibrations evident on the drag interaction on lift trace, were due to the various components of the drag linkage.

5.4. Natural frequencies.

The natural frequencies of the balance plus various weights of models were obtained on the calibration stand by using an audio-frequency oscillator driving a permanent magnet loudspeaker which was placed on the top support plate. The outputs of the balance were displayed on an oscilloscope with the following results

Model	Weight gms	Lift	Moment	Drag
No model	zero	350 c/s	3,500 c/s	2,600 c/s
10° plain delta $AR = 1$	73·3	230 c/s	345 c/s	> 2,000 c/s
10° caret delta „	66·6	220 c/s	230 c/s	„
6° plain delta „	43·8	270 c/s	360 c/s	„

11

The proximity of the moment natural frequency to that of lift for the 10° caret delta indicated a possible difficulty which the tests confirmed. There was considerable mechanical coupling resulting in extremely high oscillatory moment loads. The two frequencies were just sufficiently de-coupled by reducing the model inertia in pitch. A similar coupling occurred with the 20 cone which had been tested on the MK 2 balance[7] and as it was not possible to separate the frequencies in this case, it could not be tested on the MK 3 balance.

5.5. *Filter Attenuation and Response.*

The characteristics of the low-pass filters were checked by recording their response to a step input. Since the minimum running time available was 28 ms (36 ms and 44 ms for the two test conditions) the filters were adjusted to record within 1 per cent of the true value in less than 18 ms in order to give a minimum of 10 ms steady trace. The attenuation of these filters was negligible.

The addition of the notch filters (Section 4) reduced the response and so the low-pass filters were changed in order to keep the overall response about the same. These adjustments were made between test runs and judged on the results so that the exact response time was not known but as the test conditions gave greater than minimum running time, it was felt that there was a sufficient margin. The attenuation of the notch filters was 0·2 per cent.

5.6. *Tare Calibrations.*

Recordings were taken both with wind-off and with no model on the balance. In the former case the nozzle throat was replaced by a plug while in the latter case a slender cone and wedge were separately supported in front of the balance sting. Fig. 12 shows the resulting traces for the test conditions.

This calibration was incorporated in the reduction of the test results by drawing a mean line through the record and measuring the correction at a given time from the start of the run. Readings were then taken at this standard point for all test runs.

The oscillation visible on the trace of Fig. 12 was caused by movement of the complete working section, probably relative to the dump tank. Its amplitude was reduced by a modification which eliminated the friction between the nozzle and working section but the residual oscillation still made accurate reading of the drag trace difficult.

The balance centre of rotation was virtually on the tunnel centreline where disturbances were at a maximum (*see* Section 2.2). This arrangement was preferred as variations could arise from parts of models moving into the central region with incidence. To check whether the disturbances averaged themselves out over the models, several readings were repeated at different positions from the nozzle exit. There were no variations that could be seen above the general experimental scatter.

5.7. *Hemisphere Check.*

An additional check on the drag channel under dynamic conditions was carried out by measuring the drag of the hemisphere which was used on the MK 2 balance (*see* Ref. 7) under the same tunnel conditions. The resulting value of drag coefficient was within 2 per cent of that previously obtained and within 2 per cent of the theoretical value of 0·92.

6. *Performance and Accuracy.*

6.1. *Performance.*

The performance of the balance is summarized below:

Characteristic	Lift	Drag	Pitching moment
Design max. load	50 lb	50 lb	50 lb in
Reserve factor (proof)	3·5	> 5	2

Characteristic	Lift	Drag	Pitching moment
Sensitivity at 3V excitation (approx.) (*see* Section 5.2)	3·6 mv/lb	1·8 mv/lb	5 mv/lb in
Interaction—static	−0·8% drag	−0·9% lift	0
Interaction—dynamic	−0·9% drag	−2 to −2·5% lift	0
Natural frequency—no models	350 c/s	3,500 c/s	2,600 c/s
Natural frequency—design models	220 – 270 c/s	> 2,000 c/s	230–360 c/s
*Accuracy (*see* below)	±7·5%	±10·5%	±4%
Incidence range	±30°		
Model base	0·3 in dia. min.		

6.2. *Accuracy.*

Errors could arise from the various sources tabulated below. They fall into several categories, i.e. random errors, consistent errors, those that vary with the applied loads and those that do not.

SOURCE OF ERROR	NORMAL FORCE		AXIAL FORCE		MOMENT	
	Random	Consistent	Random	Consistent	Random	Consistent
Static calibration	—	±1%	—	±2·5%	—	±1%
Temperature correction	±0·5%	—	±1%	—	±0·5%	—
Trace reading	±3%	—	±3%	—	±3%	—
Lag effect	—	±2%	—	±2%	—	±2%
Oscilloscopes	±1%	—	±1%	—	±1%	—
Interaction	—	—	—	±0·2% lift	—	—
Tare loads	—	—	—	±0·005 q lb	—	—
TOTAL	±4·5%	±3%	±5%	±4·5% ±0·2% lift ±0·005 q lb	±4·5%	±3%

The maximum errors for any test condition will evidently depend on the test conditions, model and incidence and can be obtained by using the errors tabulated above. These errors have been calculated for five typical cases and are given below:

---

*For max. design loads. Total of maximum possible random and consistent errors.

Case 1. $6°$ plain delta $AR = 1$ $R_e = 3·5 \times 10^6$ at $\left(\dfrac{L}{D}\right)$ max.

2. $6°$ plain delta $AR = 1$ $R_e = 3·5 \times 10^6$ at $12°$ incidence

3. $10°$ plain delta $AR = 1$ $R_e = 0·9 \times 10^6$ at $\left(\dfrac{L}{D}\right)$ max.

4.   Hemisphere at $R_e = 3·5 \times 10^6$

5.   At balance max. design loads.

Max. possible errors for	Case 1	Case 2	Case 3	Case 4	Case 5
Lift, random	$\pm4·5\%$	$\pm4·5\%$	$\pm4·5\%$	—	$\pm4·5\%$
Lift, consistent	$\pm3\%$	$\pm3\%$	$\pm3\%$	—	$\pm3\%$
Drag, random	$\pm5\%$	$\pm4·5\%$	$\pm5\%$	$\pm5\%$	$\pm5\%$
Drag, consistent	$\pm17\%$	$\pm10\%$	$\pm14\%$	$\pm4·5\%$	$\pm5·5\%$
C.P. position, random	$\pm0·4\%$	$\pm0·4\%$	$\pm0·4\%$	—	$\pm2·5\%$
C.P. position, consistent	$\pm0·3\%$	$\pm0·3\%$	$\pm0·3\%$	—	$\pm1·5\%$
Lift/drag ratio, random	$\pm9·5\%$	$\pm9\%$	$\pm9·5\%$	—	$\pm9·5\%$
Lift/drag ratio, consistent	$\pm20\%$	$\pm13\%$	$\pm17\%$	—	$\pm8·5\%$

The probable error of results, arising from random errors, depends on the number of data points from which an average is taken. The above figures represent maximum errors and are not too likely even for a single point.

6.3. *Some Results Obtained with the Balance.*

Figs. 15 to 18 show some of the results obtained with the balance while the dimensions of the corresponding models are shown in Fig. 14. Axial drag measurements (the smallest forces) for two extremes of available Reynolds number are shown in Fig. 15. An indication of the consistency of the results can be obtained by comparing the relative drags of the different models at the two Reynolds numbers and it will be seen that to a large extent the same pattern is followed but with smaller magnitudes for the differences at the higher Reynolds number in each case.

The nature of the problem is such that the agreement with theory is not easily demonstrated except with a rather detailed analysis which can be found in Ref. 9. However, it is possible to isolate the skin friction plus base drag, an even smaller force, by subtracting the pressure drag using a theoretical but reasonably accurately predictable division between upper and lower surface pressures together with the measured normal force. This has been done and the result for two models is shown in Fig. 16.

One model (No. 4) at one Reynolds number was chosen for repeated testing as a continuing check on the tests and on the consistency of the balance. The results can be seen in Fig. 16b and in view of the smallness of the force, the consistency is impressive.

Figs. 17 and 18 show that the same consistency was obtained for lift and centre of pressure position, the sensitivity in the latter case being particularly high.

7. *Discussion and Conclusions.*

In general, the design concepts outlined in the introduction were vindicated by the results. The balance gave good sensitivity and repeatability and hence would also have given good absolute accuracy if the difficulties of calibration had not arisen.

The difficulties of calibration arose from the need to have taper pinned, load carrying members, which in turn were made necessary by high interactions and high sensitivity of the supporting structure to aerodynamic loading. The root of the trouble was that the supporting structure had insufficient margin of stiffness over the sensing elements and indeed it would be difficult to achieve the required stiffness because of the high stiffness of the tension links. Some improvement could be effected by redesign of the supporting structure, e.g. by making the balance fill the space up to the incidence gear arms and by reducing the overall length of the sting beam in the balance.

However, the drag sensor was both unnecessarily stiff and unnecessarily strong, due to the impracticability of producing thinner tension links, and hence in this application a considerable improvement could probably be achieved by reverting to a cantilever for this channel.

In assessing the possible errors of Section 6.2 it should be noted that in the worst case, the measured drag was 0·25 per cent of the design maximum load. Thin, high lift/drag ratio wing, considerably increase the problems of gun tunnel balances. The high design strength was necessary because of starting and vibrating loads, the wide range of possible conditions and models and because of handling considerations.

Taken overall, the balance performed very well and some excellent results were obtained, proving the basic concept. With a few minor improvements, the remaining problems could be overcome to produce a totally satisfactory balance.

8. *Acknowledgements.*

REFERENCES

No.	Author(s)	Title, etc.
1	I. M. Hall	Transonic flow in two-dimensional and axially-symmetric nozzles. A.R.C. 23 347. 1961.
2	B. Stratford and G. S. Beavers	The calculation of the compressible turbulent boundary layer in an arbitrary pressure gradient—a correlation of certain previous methods. A.R.C. R. & M. 3207. 1959.
3	D. A. Needham	Progress report on the Imperial College Hypersonic Gun Tunnel. Imperial College of Science and Technology. Aeronautics Dept. Tech. Note No. 118. 1963.
4	H. H. Album	Flow inclination measurements in hypersonic tunnels. *Jn. AIAA* Vol. 2, No. 1, January, 1964, p. 104.
5	L. Penneligion, R. F. Cash and M. Shilling	Free flight tests in the NPL 6 in. (15 cm) shock tunnel of model HB-2 using multiple spark recording. A.R.C. C.P. 934. 1966.

REFERENCES—*continued*

No.	Author(s)	Title, etc.

6 R. MacArthur and J. F. Martin

Use of field effect transistors in shock tunnel instrumentation circuits.
Proceedings of 2nd International Congress on Instrumentation in Aerospace simulation facilities. Arnold Air Force Station, Tennessee, U.S.A.

7 T. Opatowski .. .. ..

Gun tunnel measurements of lift, drag and pitching moment on a 20° cone, a plain delta and a caret delta wing at a Mach No. of 8·3.
A.R.C. C.P. 908, 1965.

8 L. Pennelegion and G. S. Smith

Millisecond measurements of aerodynamic Forces in a high pressure shock tunnel.
NPL Aero Report 1120.
A.R.C. 26 309, 1964.

9 T. Opatowski .. .. ..

An experimental study of the flow around and the forces developed by hypersonic lifting vehicles.
Ph.D. Thesis, London University, September, 1967.

Figure shows ΔM, where M = 8 + ΔM

Top
3″

2″

1″

Centre line

1″

2″

3″

Flow direction

Nozzle exit plane   1″   2″   3″   4″   5″   6″   7″   8″ Aft.

ΔM ——→ 1″ = 1 (measured horizontally or vertically)
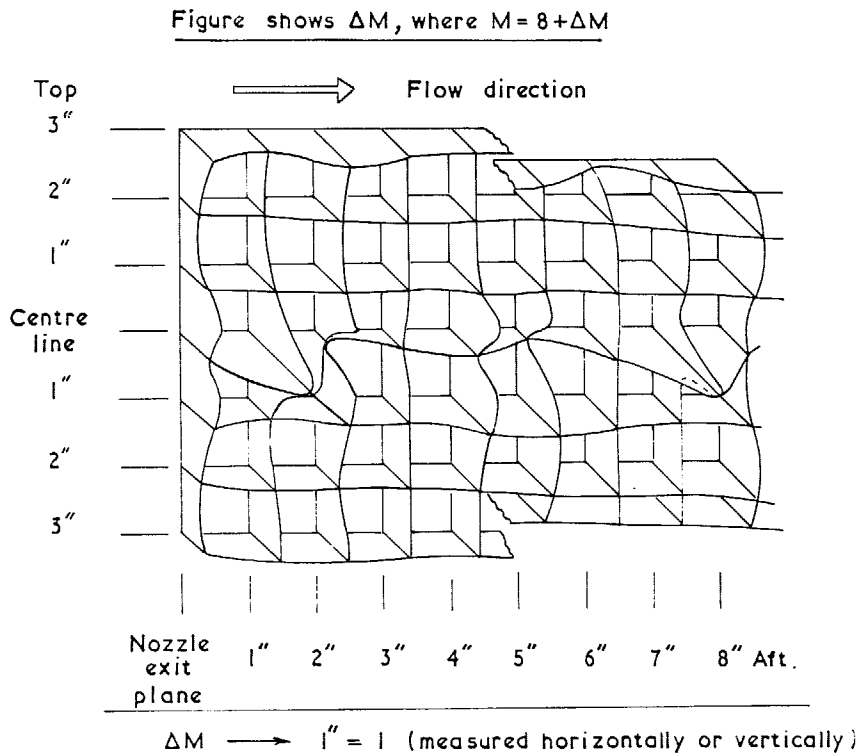
FIG. 1a.   Mach No. distribution in the tunnel on the vertical centre section.

Figure shows ΔM where M = 8 + ΔM

Flow direction into paper

Top
3″

2″

1″

₵

1″

2″

3″

ΔM ——→ 1″ = 1, (from M = 8 base line)

Cross section at 3″ aft of nozzle exit plane

Pt.   3″   2″   1″   ₵   1″   2″   3″   Stbd.
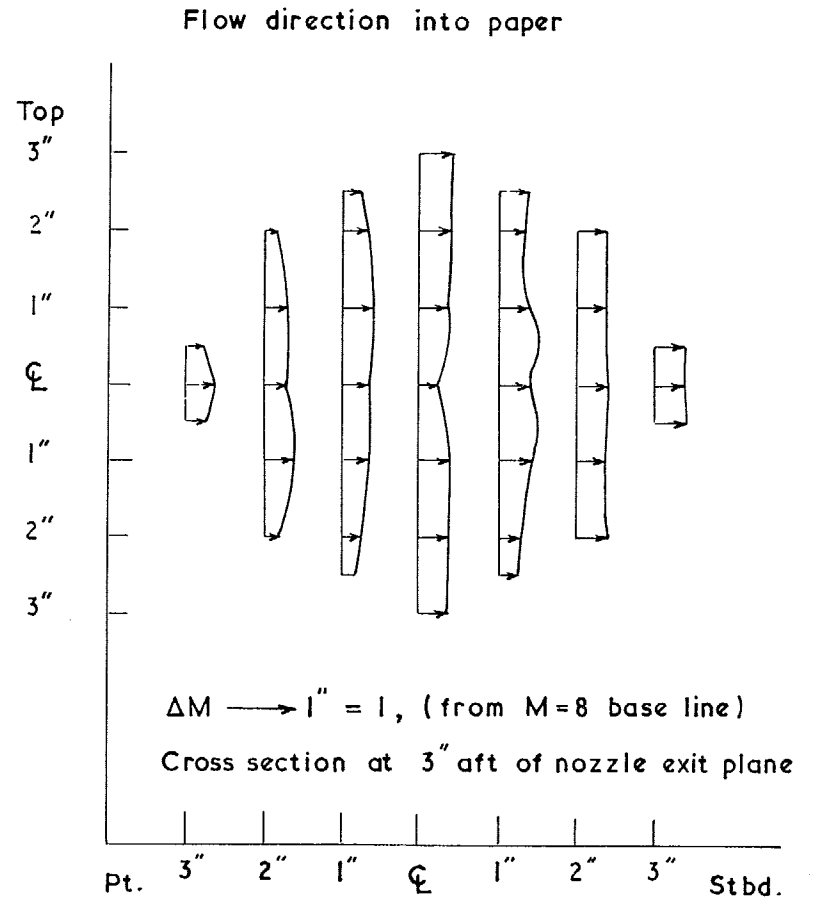
FIG. 1b.   Mach No. distribution in the tunnel. Lateral cross section.

Pitot
pressure
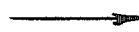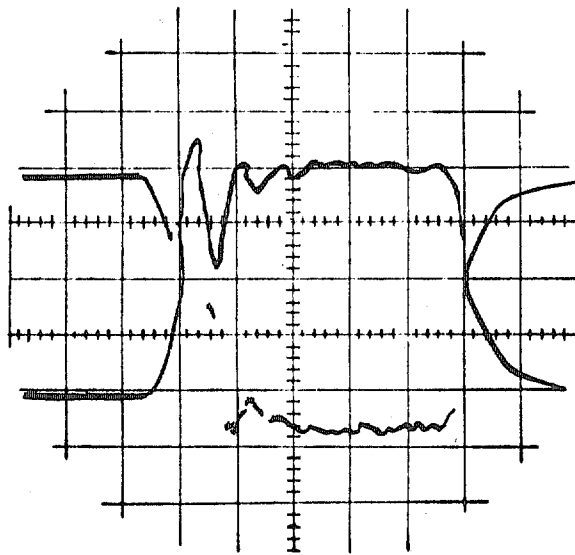
$\longrightarrow$ 10msec/cm

(a)   Normal

Pitot
pressure
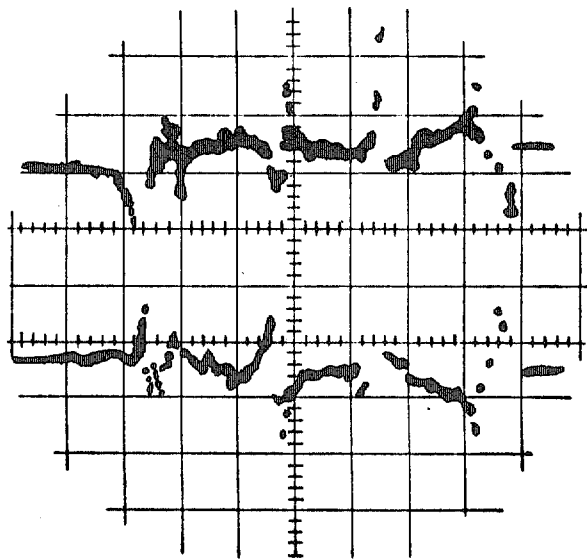
$\longrightarrow$ 10msec/cm

(b) With pressurized barrel.

FIG. 2.   Tunnel calibration; typical traces.

18
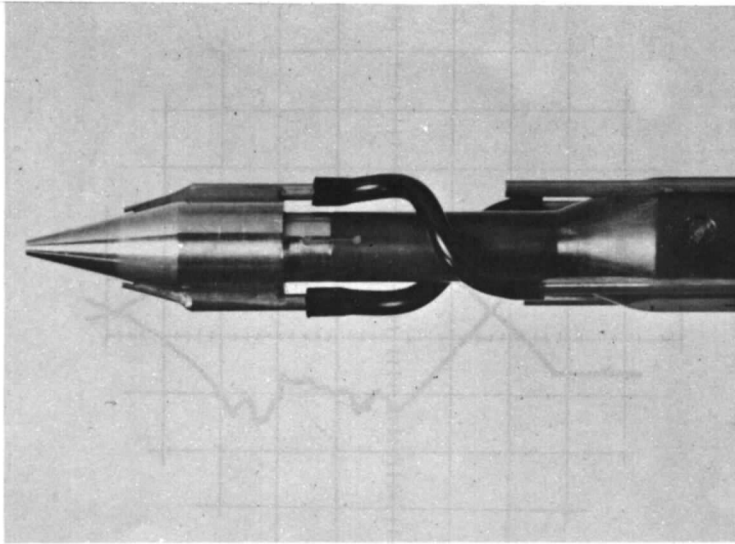
(a)   Sensing head
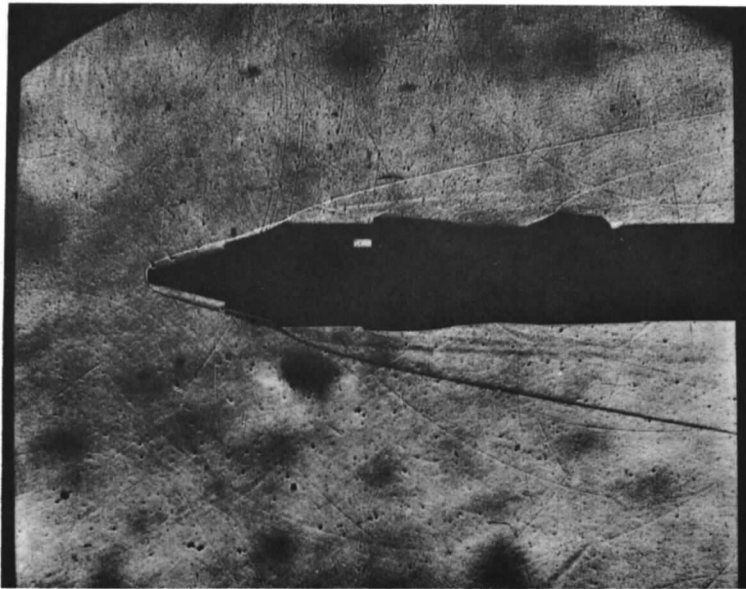
(b)   Schleiren photograph of flow

FIG. 3 a & b.   The 'pressure recovery' flow inclination probe.
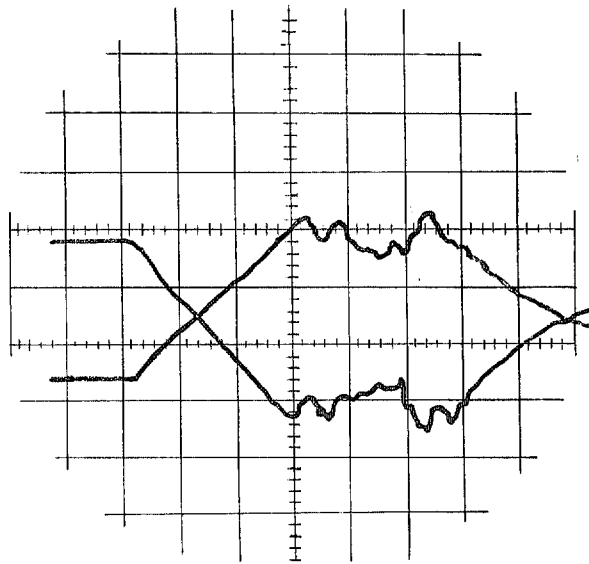
FIG. 3c.   Typical flow inclination probe trace.
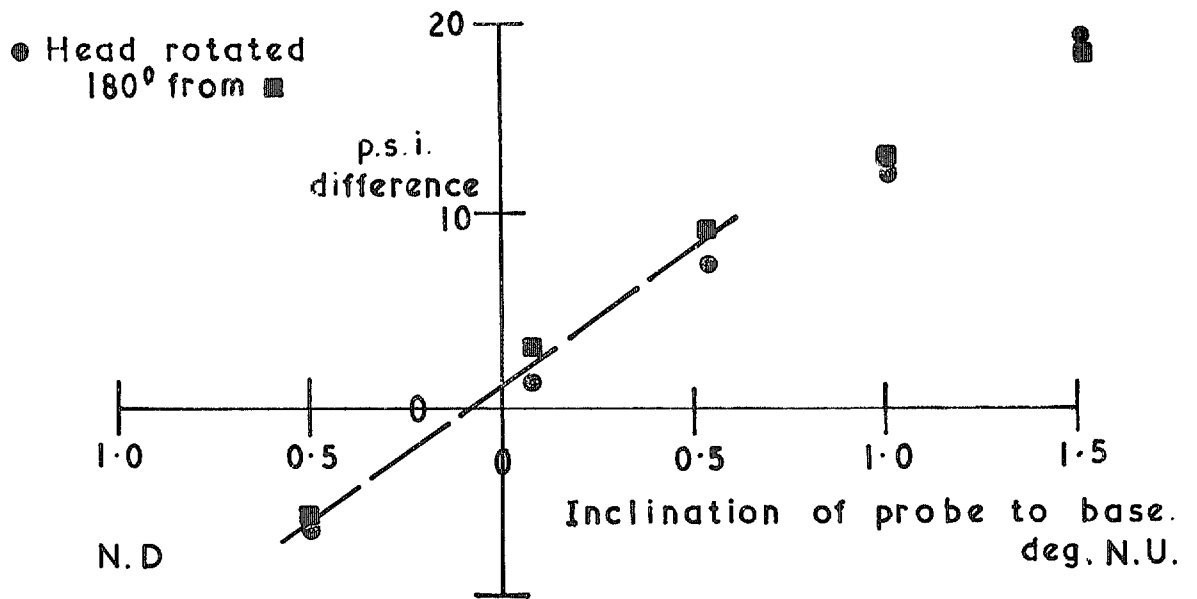
FIG. 4.   Results of flow inclination probe measurements at 1 in below centreline.
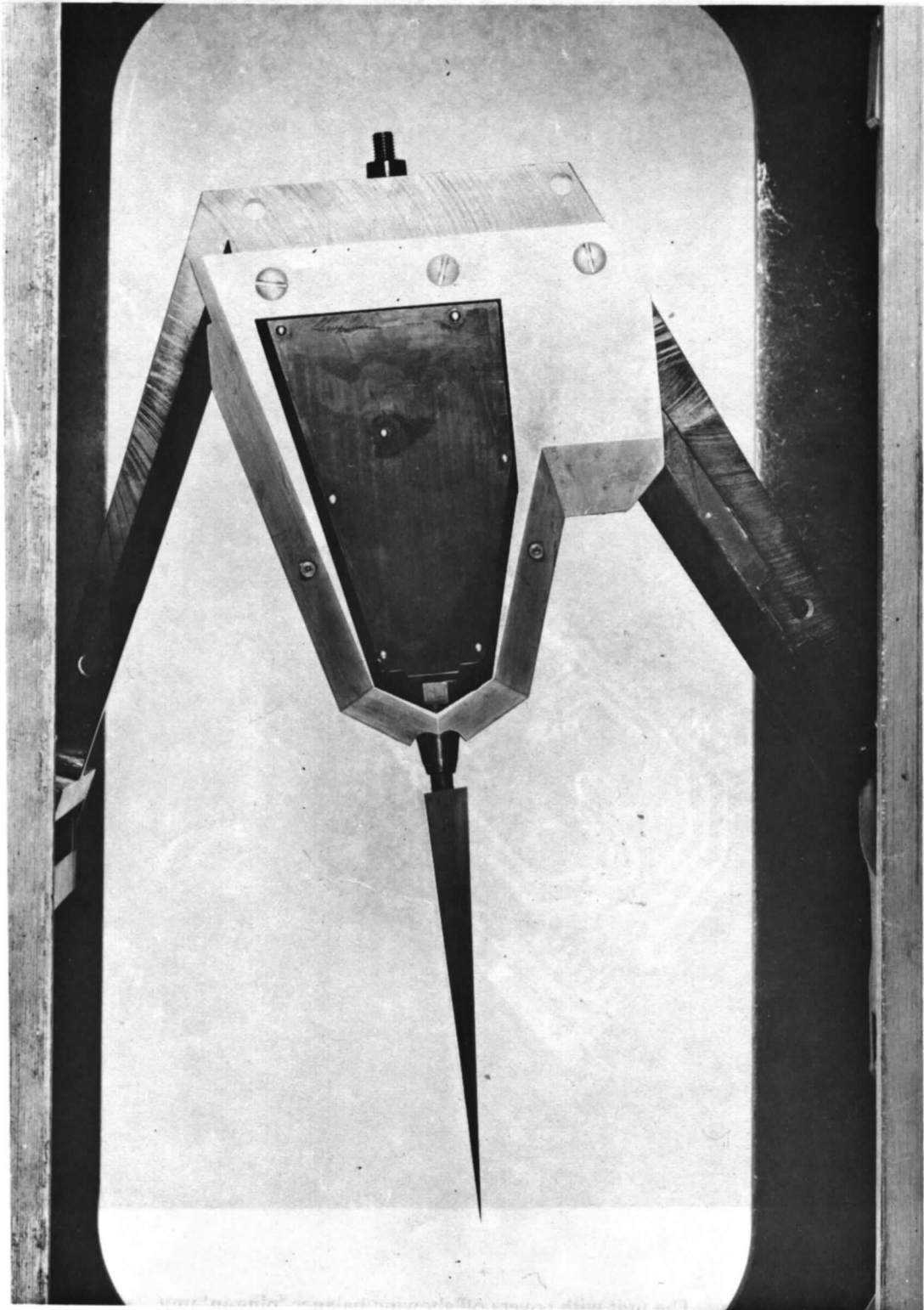
FIG. 5.   The Mk III balance and a model in the tunnel.
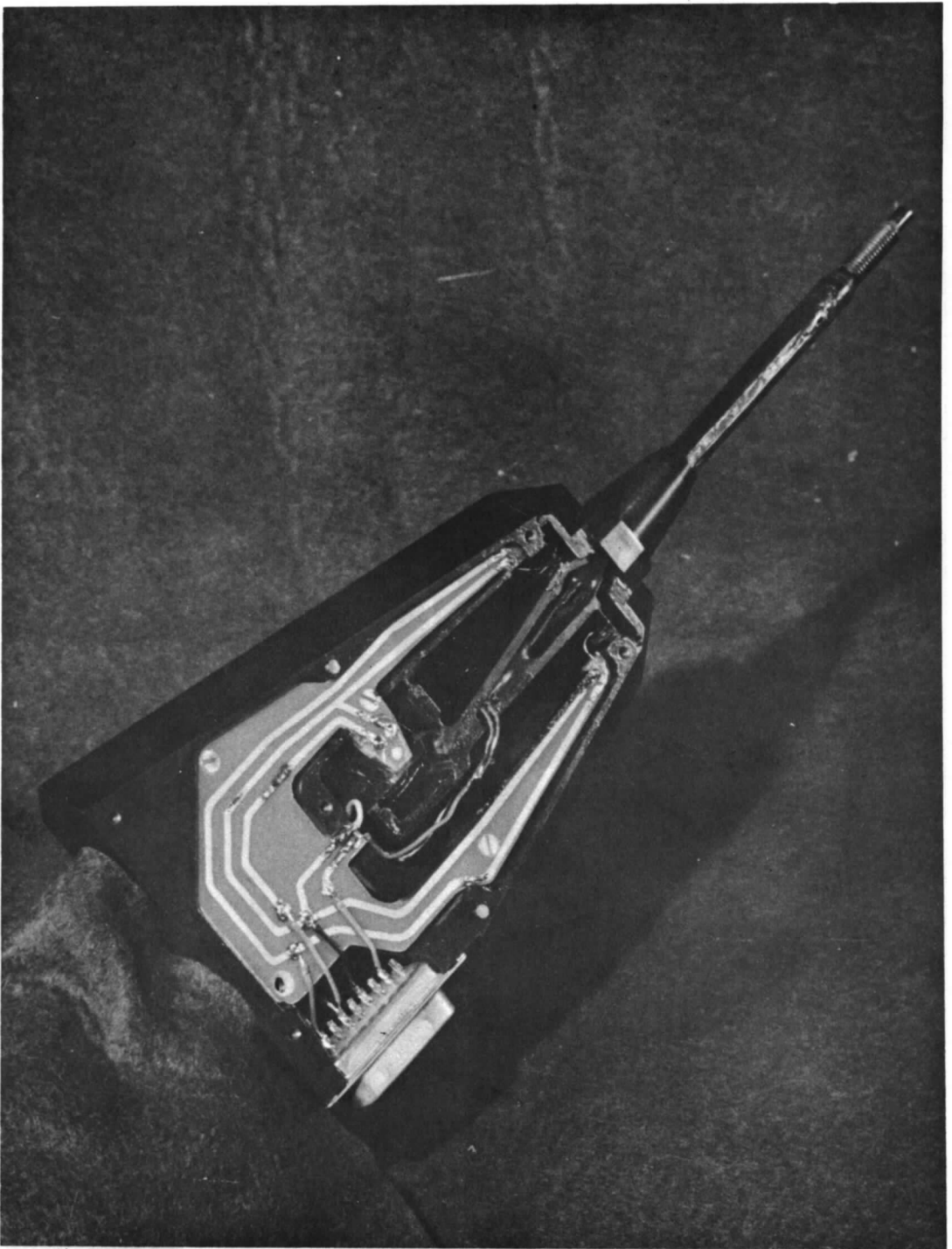
FIG. 6a. The unit with covers off showing balance 'plug-in' unit.
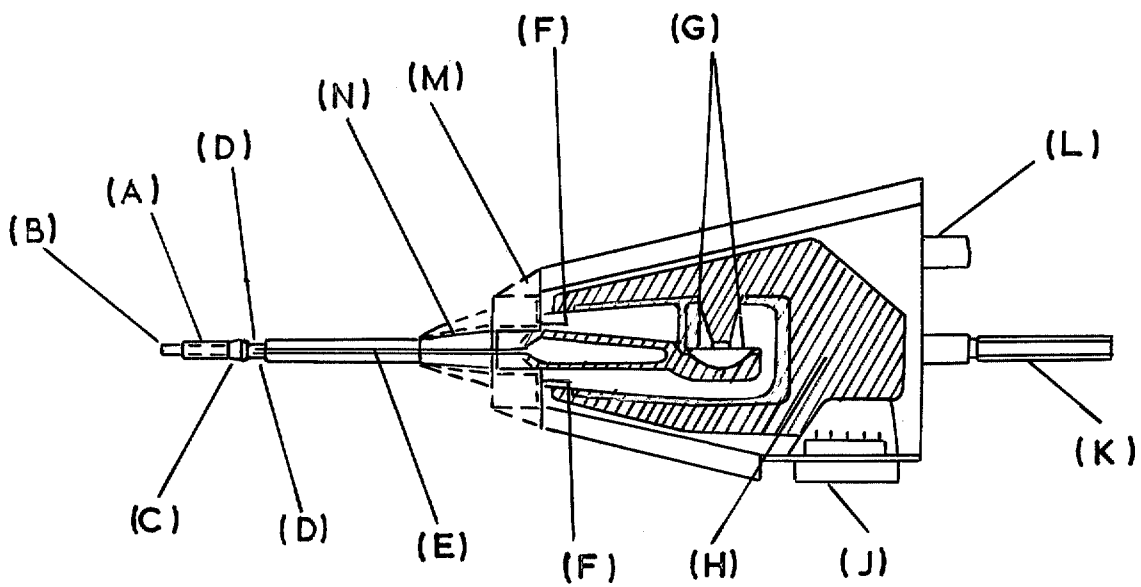
½ Scale.   Gauges at (D),(F) and (G) .

FIG. 6b.   The balance 'plug-in' unit. General arrangement.
(Described in Section 4.1. of text).

4 gauges measuring
lift

Gauge top and bottom
measuring pitching moment
by bending of beam

Idler link reacting
lift load and allowing
lateral movement

Model attached
here

Two links 0·010″ thick
taking tension and
compression only

0·010″ thick links
top and bottom taking
tension and compression
and allowing some lateral
movement

4 gauges measuring
drag
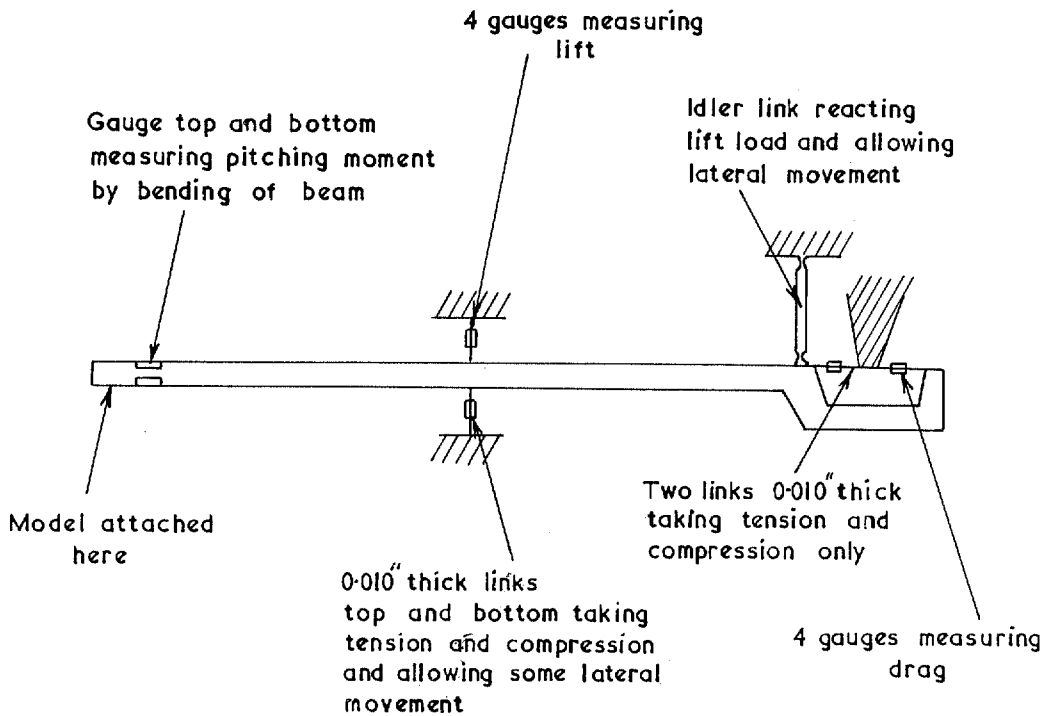
FIG. 6c.   Layout of sensing elements.

Upper and lower plates slide in existing tracks
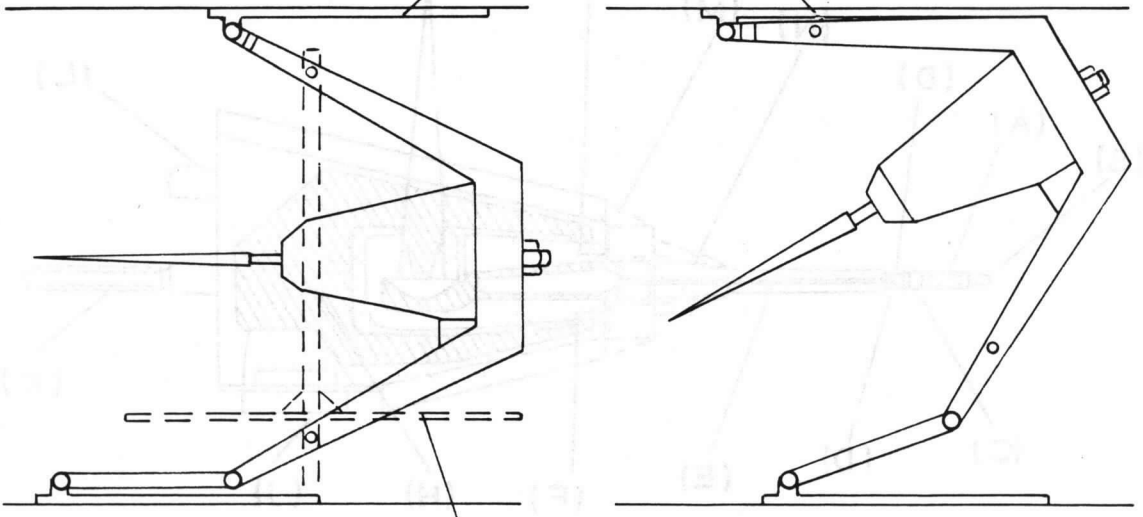
Incidence setting attachment

Zero incidence

30° incidence

FIG. 7a. Incidence setting and adjustment.
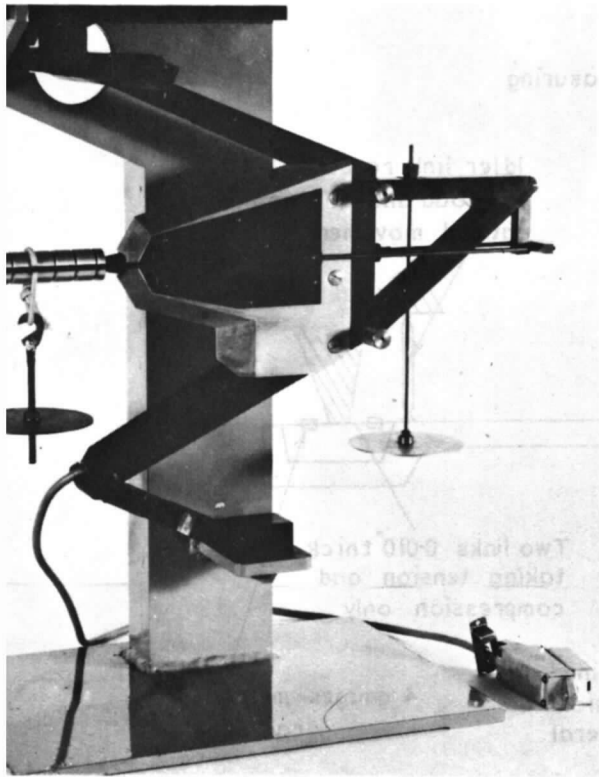
For static calibration
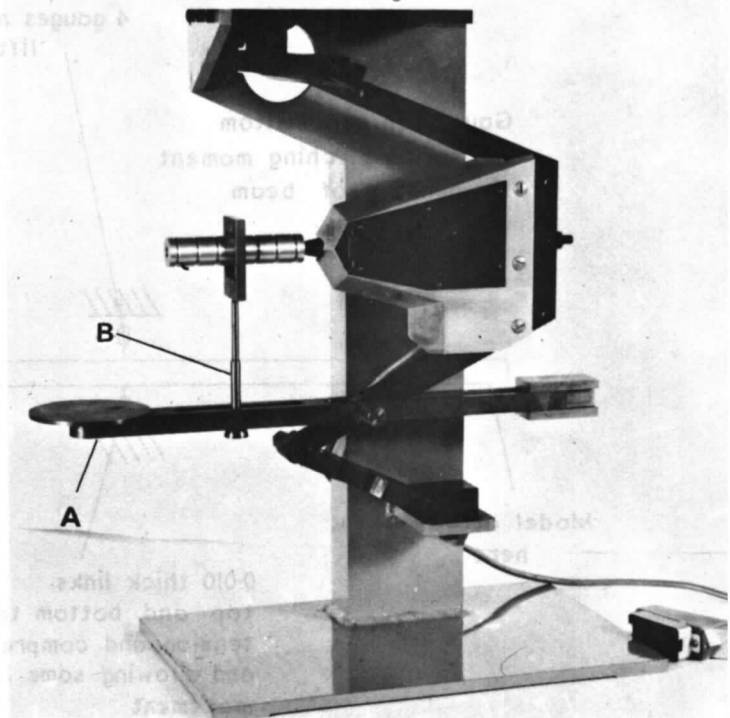
For dynamic interaction

FIG. 7b. Calibration equipment.
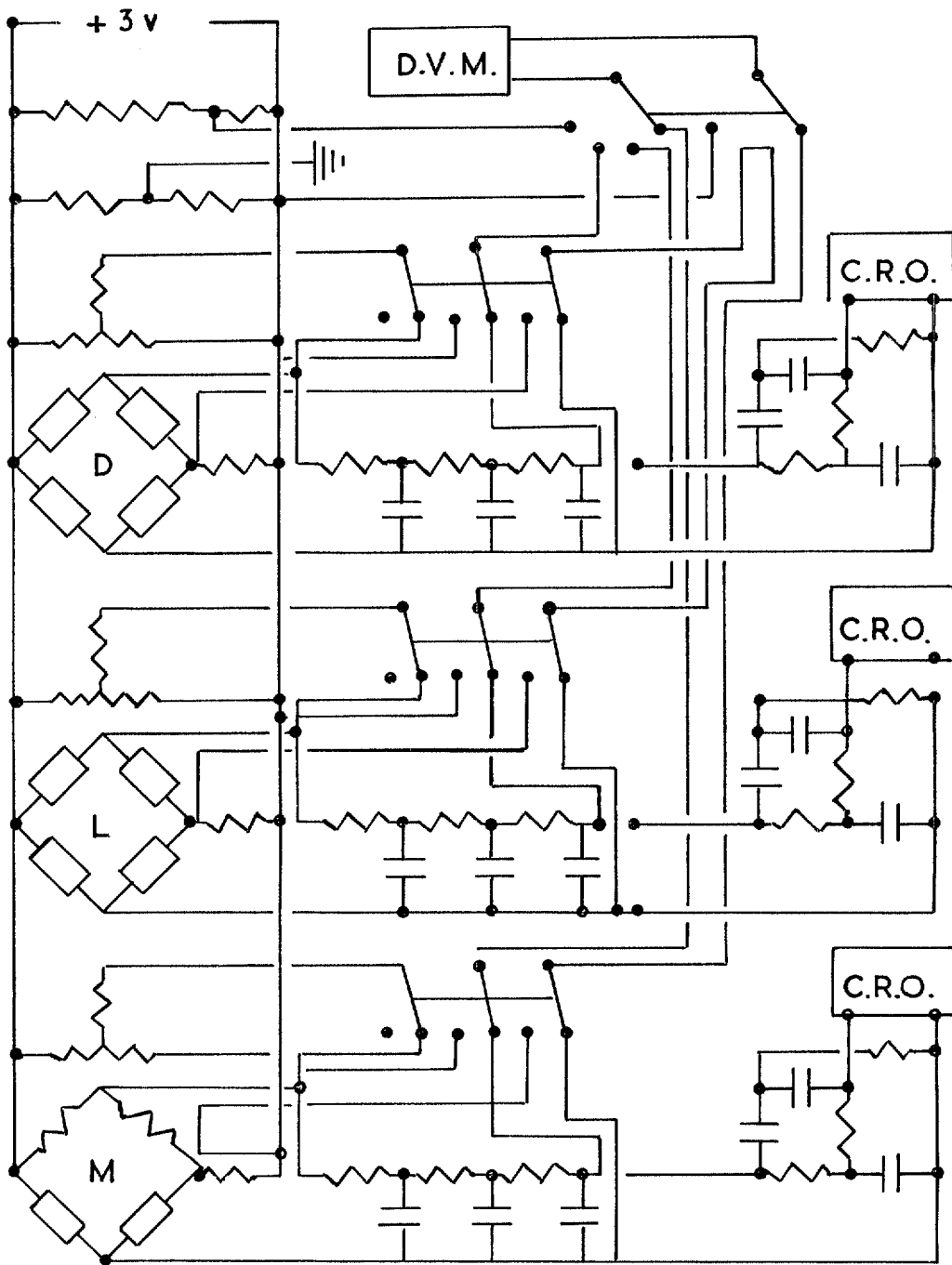
FIG. 8. Circuit diagram.

$$R_I = 2R_O \quad : \quad C_O = 2C_I$$
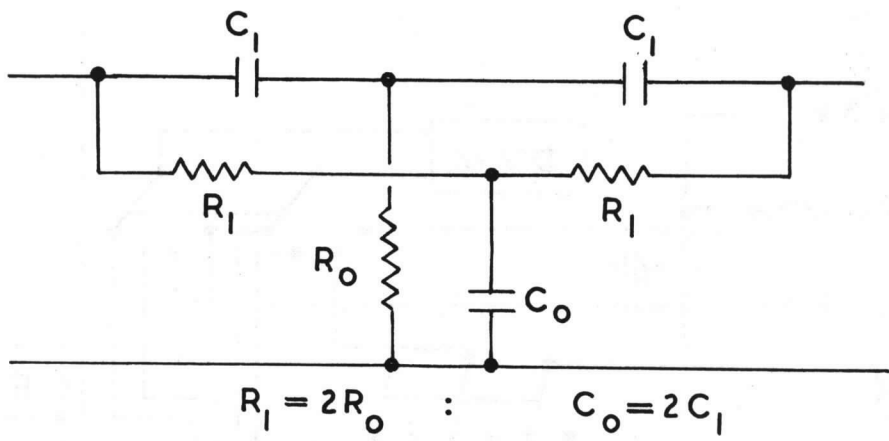
(a)   Circuit
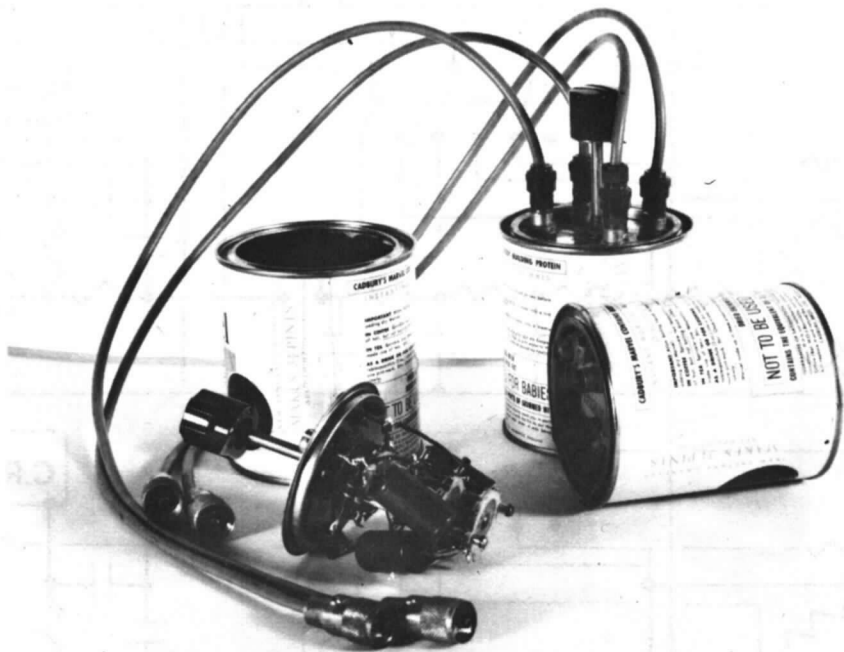
(b)   Photograph of units

FIG. 9 a & b.   The 'parallel T' filters.
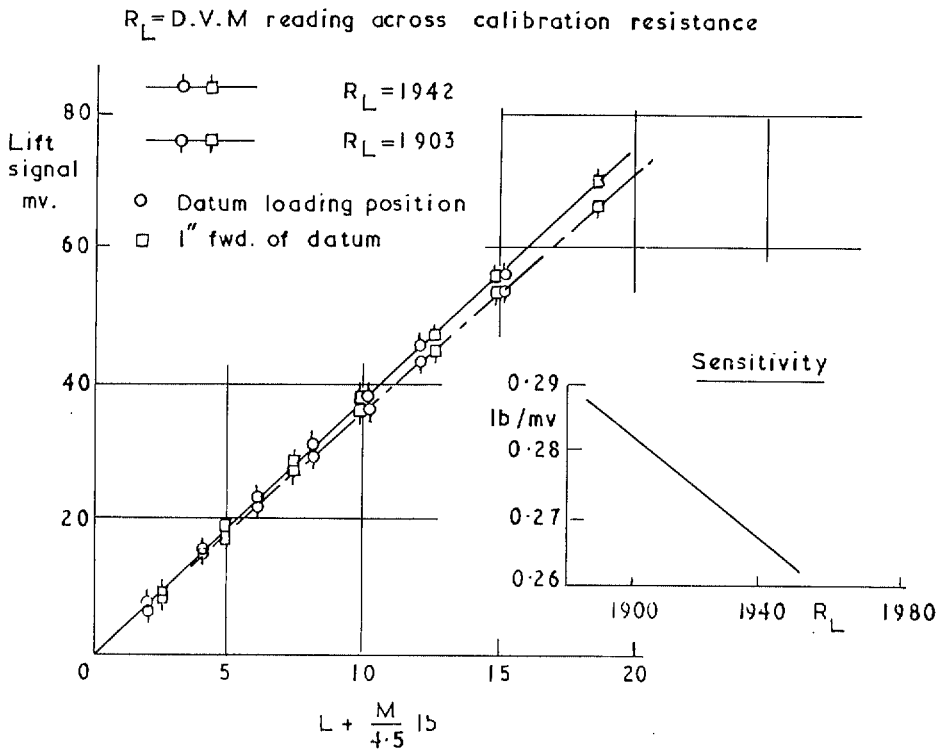
FIG. 10a.   Lift: static calibration.
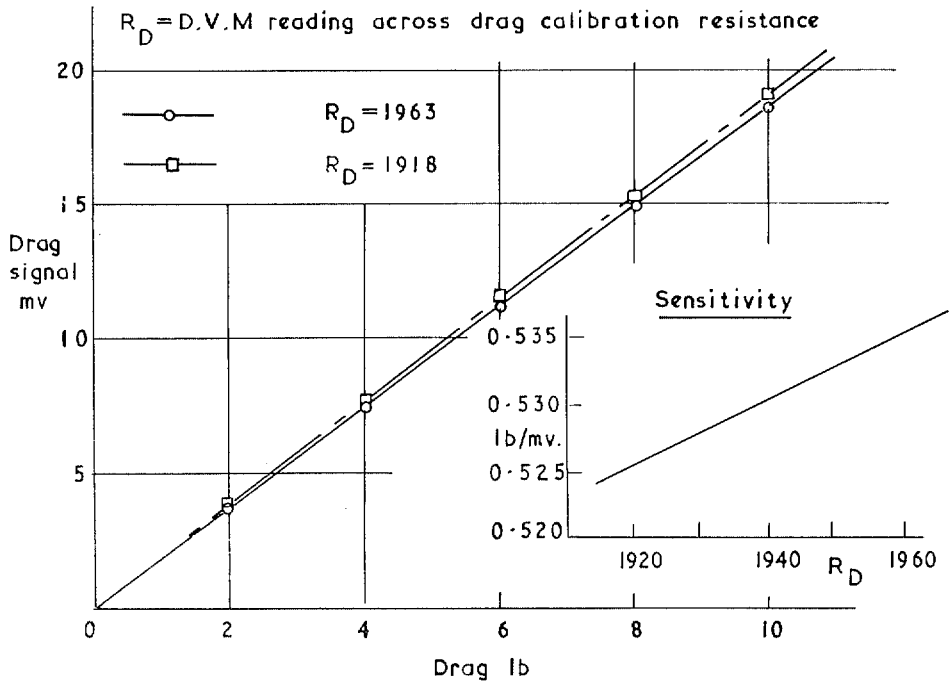
FIG. 10b.   Drag: static calibration.
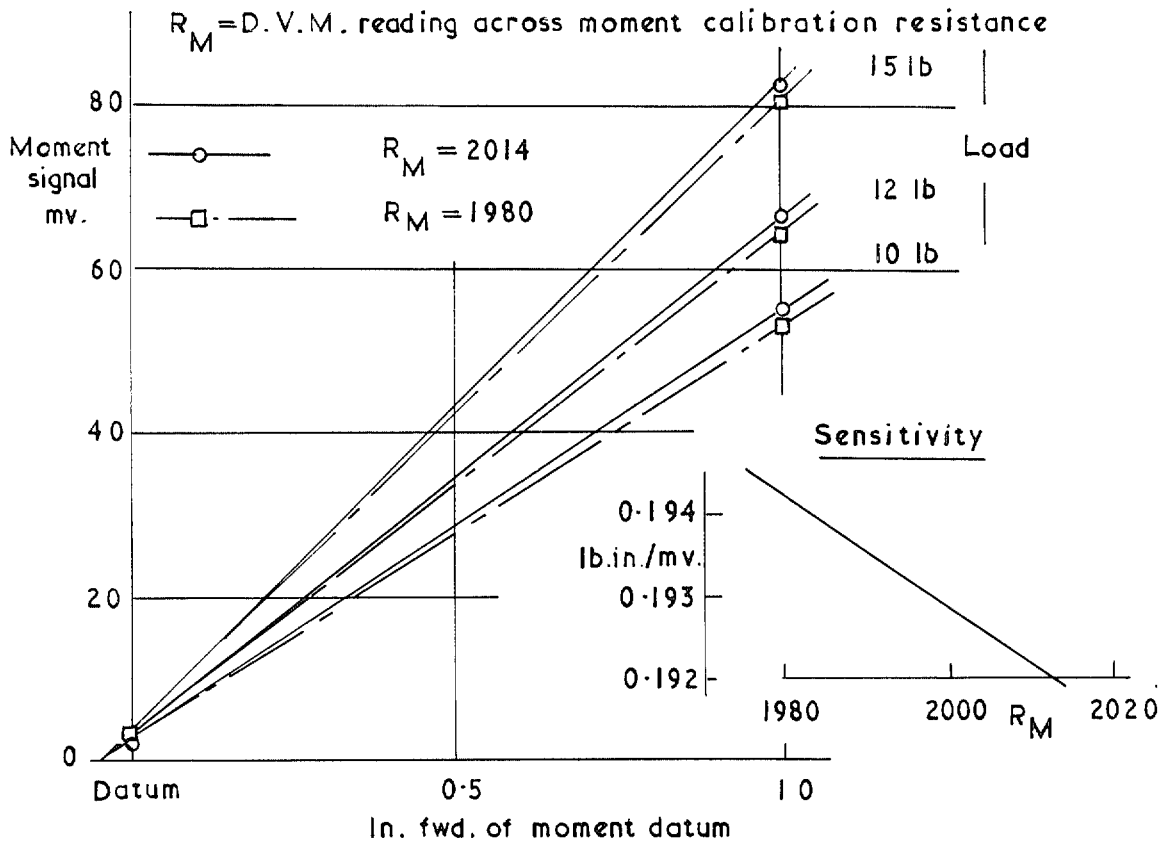
FIG. 10c.   Pitching moment: static calibration.

Drag
200μv/cm
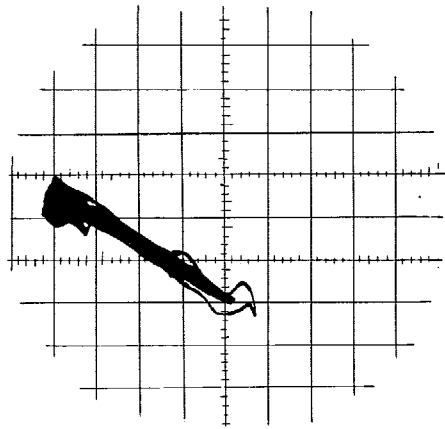
Lift 10 mv/cm →

(a) Lift on drag.

Drag
2 mv/cm ↑

Lift 200 μv /cm

(b) Drag on lift.

FIG. 11. Dynamic interaction: typical traces.
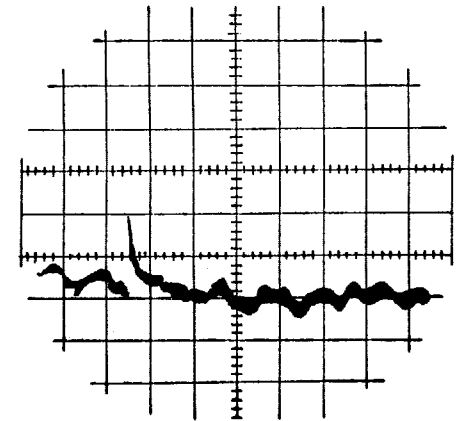
Drag
200 μv / cm
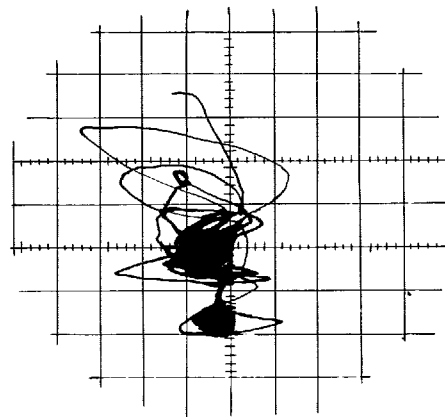
→ 20 msec /cm.

Conditions for Re=0·9 x 10^6 runs.
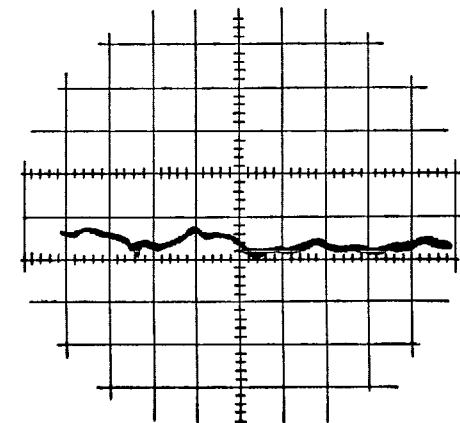
Drag
200 μv / cm

→ 20 msec/cm.

Conditions for Re = 3·5 x 10^6 runs.

FIG. 12. Tare calibration: typical traces.

Drag

Lift

20 msec/cm
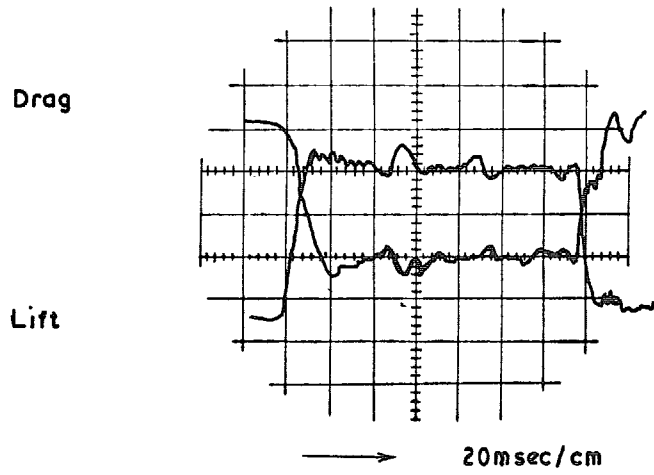
(a) Lift and drag, $R_e = 3.5 \times 10^6$

Drag

Lift

20 msec/cm

(c) Lift and drag, $R_e = 0.9 \times 10^6$
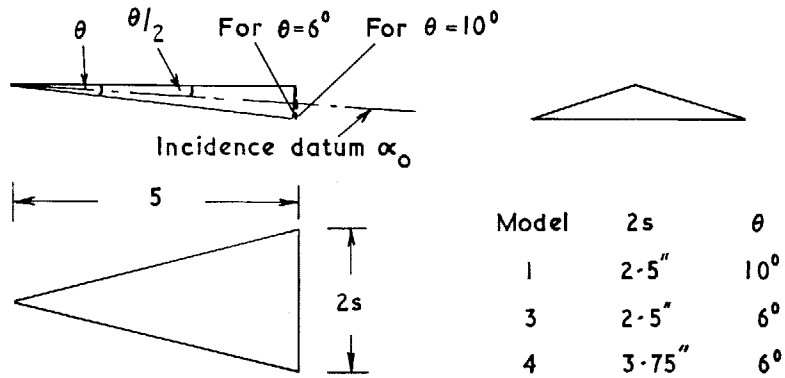
Pitching
moment

20 msec/cm
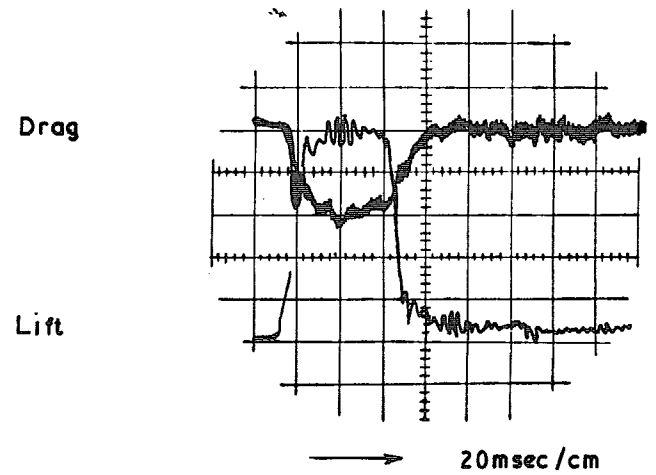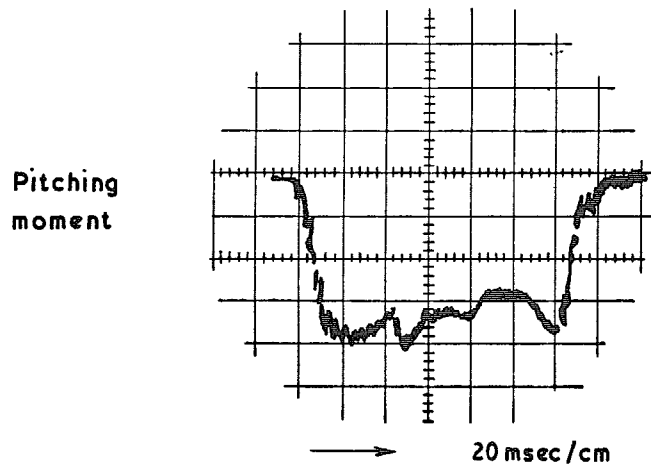
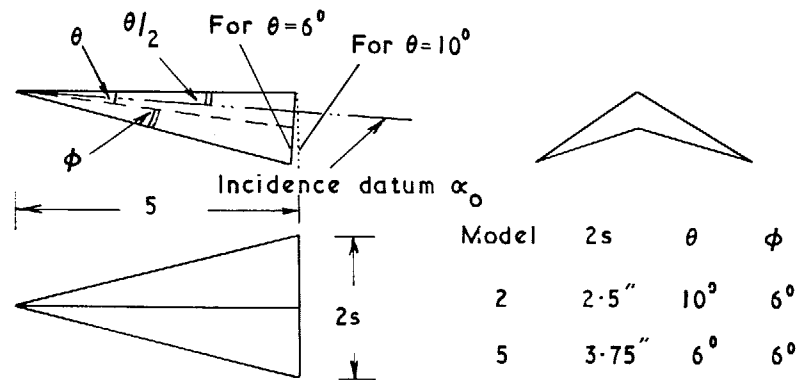(b) Pitching moment, $R_e = 3.5 \times 10^6$

Drag

20 msec/cm
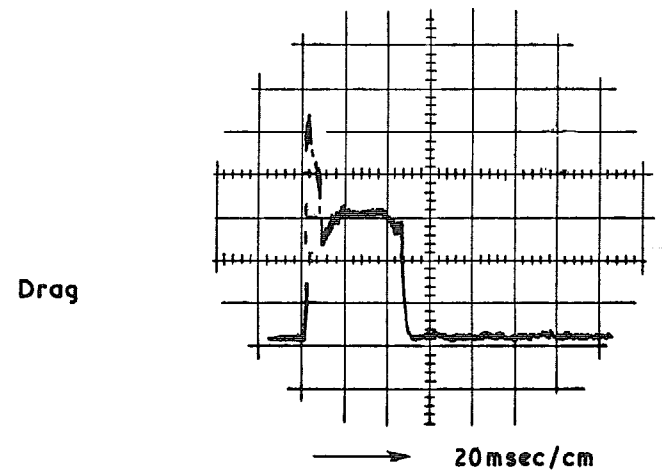
(d) Hemisphere drag

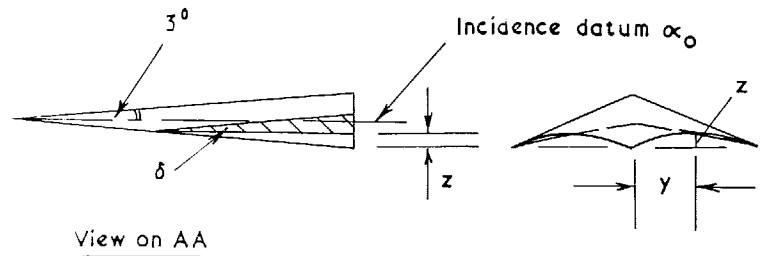FIG. 13 a & b. Force measurement: typical
traces. $M = 8.3$.

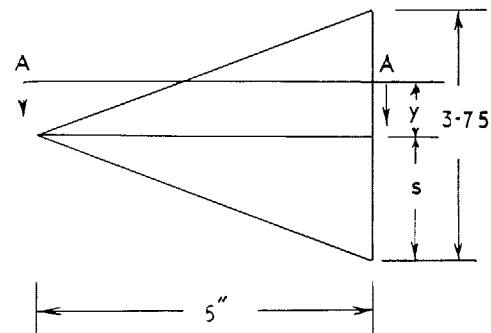FIG. 13 c & d. Force measurement: typical traces.
$M = 8.3$.

θ $\theta/2$ For $\theta=6°$ For $\theta=10°$

Incidence datum α_o

5

2s

Model	2s	θ
1	2·5″	10°
3	2·5″	6°
4	3·75″	6°

(a) Plain wings

θ $\theta/2$ For $\theta=6°$ For $\theta=10°$

ϕ

Incidence datum α_o

5

2s

Model	2s	θ	ϕ
2	2·5″	10°	6°
5	3·75″	6°	6°

(b) Caret wings

FIG. 14 a & b. Model dimensions and details.

3°

Incidence datum α_o

δ

z

z

y

View on AA

A   A

Y   y   3·75

s

5″

Model 6 having same
volume as other
wings
δ varies linearly from
root to tip
Upper surfaces
are flat

y/s	0	0·1	0·2	0·3	0·4	0·5	0·6	0·7	0·8	0·9	1·0
z''	0	0·027	0·048	0·063	0·072	0·075	0·072	0·063	0·048	0·027	0
$\delta°$	6·85	6·51	6·17	5·82	5·48	5·14	4·80	4·45	4·11	3·77	3·43

FIG. 14c. Twisted wing.

Experiment   Model

+ $10°$ plain wing, AR=1   1

× $10°$ caret wing, AR=1   2

⊕ $5°$ plain wing, AR=1   3

▣ $6°$ plain wing, AR=1·5   4

◈ $6°$ caret wing, AR=1·5   5

▲ $5°$ twisted wing, AR=1·5   6

Random error $\pm$ 5% max

$M = 8·3$

Theory $(p_b = p_\infty)$

—————— Plain wings

— · — · — Caret wings
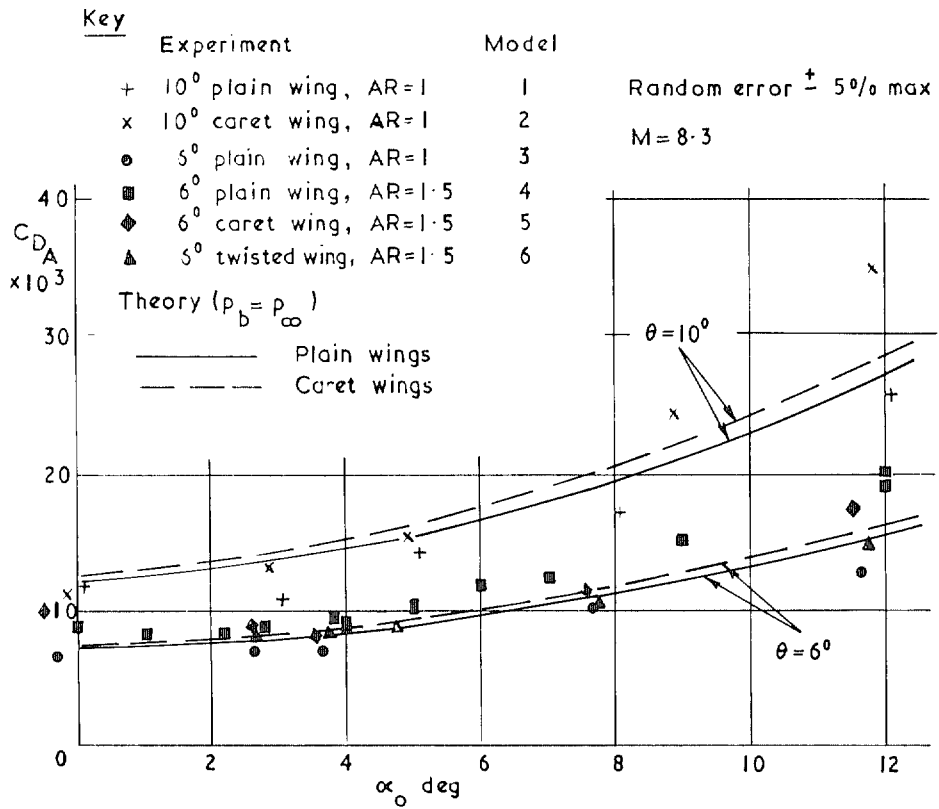
$\theta = 10°$

$\theta = 6°$

$C_{D_A} \times 10^3$

α_o deg

Fig. 15a.   Axial force coefficient, C_{D_A} vs incidence for $R_e = 0·9 \times 10^6$.

Experiment   Model

+ $10°$ plain wing, AR=1   1

× $10°$ caret wing, AR=1   2

⊕ $6°$ plain wing, AR=1   3

▣ $6°$ plain wing, AR=1·5   4

◈ $6°$ caret wing, AR=1·5   5

▲ $6°$ twisted wing, AR=1·5   6

Random error $\pm$ 5% max

$M = 8·3$

Theory $(p_b = p_\infty)$

—————— Plain wings

— — — Caret wings

$\theta = 10°$

$\theta = 6°$

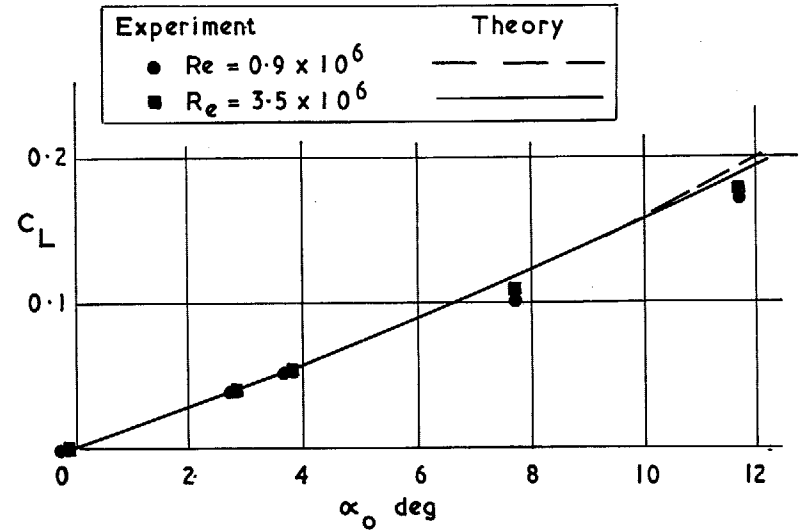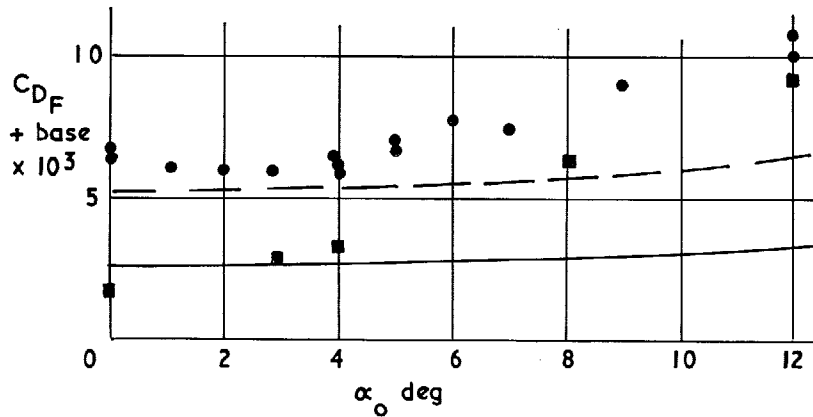$C_{D_A} \times 10^3$

α_o deg
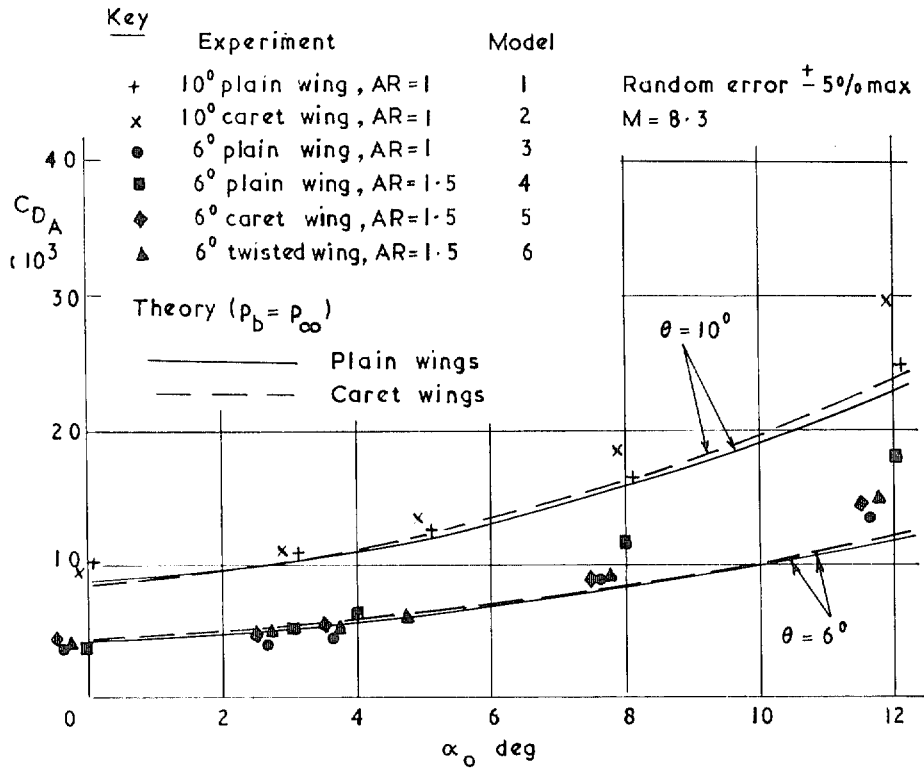
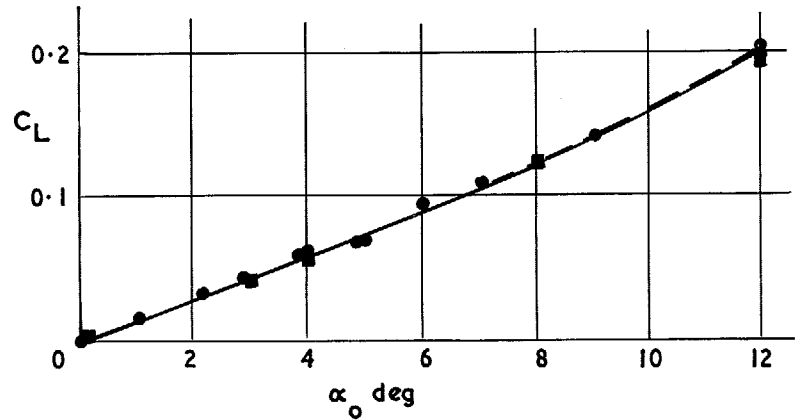Fig. 15b.   Axial force coefficient, C_{D_A} vs incidence for $R_e = 3·5 \times 10^6$.
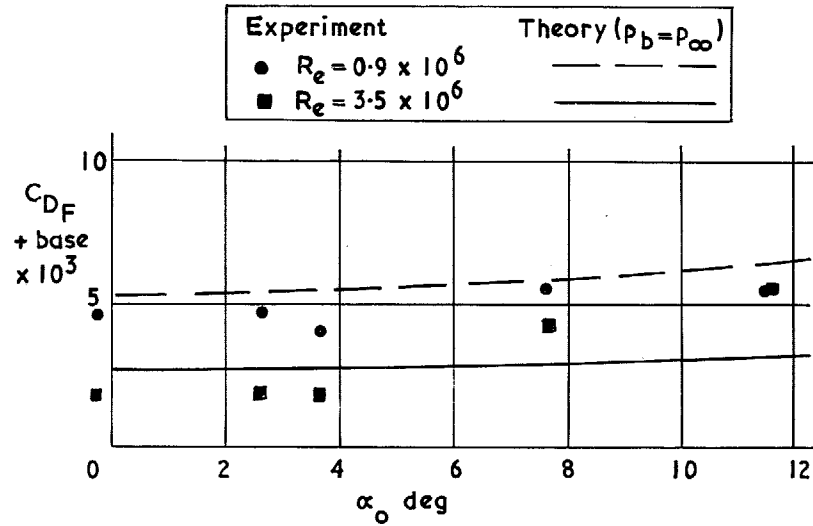
32

(a)   Model 3 , 6° plain wing, AR = 1

(b) Model 4 , 6° plain wing , AR = 1·5

FIG. 16 a & b.   Skin-friction drag.

Experiment   Theory
● R_e = 0·9 x 10^6
■ R_e = 3·5 x 10^6

(a)   Model 3 , 6° plain wing, AR = 1

(b) Model 4, 6° plain wing, AR = 1·5

FIG. 17 a & b.   Lift.

Key

+ 10^0 plain wing, AR = 1   ▣ 6^0 plain wing, AR = 1·5

× 10^0 caret wing, AR = 1   ◆ 6^0 caret wing, AR = 1·5

● 6^0 plain wing, AR = 1   ▲ 6^0 twisted wing, AR = 1·5

(a) $R_e = 0.9 \times 10^6$

(b) $R_e = 3.5 \times 10^6$

α_o deg
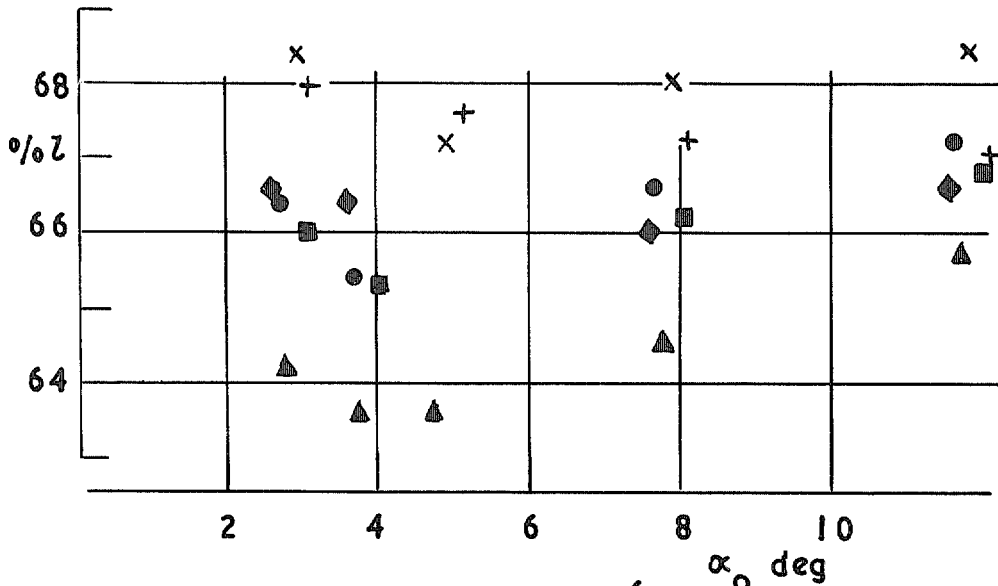
FIG. 18 a & b.   Centre of pressure position *vs* incidence.